博士論文

Optical Manipulation of Two-dimensional Colloidal Nanomaterials
（二次元ナノ物質の光操作）

平成 30 年 3 月

富永　亮

山口大学大学院医学系研究科

CONTENTS

Chapter 1. Introduction

1-1. Radiation Pressure of Light

1-1-1. Optical Manipulation of Spherical Colloidal Particles

A photon carries not only energy but also momentum. When the photon impinges on a colloidal particle, the momentum of the impinged photon changes owing to light scattering including reflection, light absorption, or refraction as shown in Figure 1-1. At that time, radiation pressure is exerted on the particle as a reaction force by the law of conservation of momentum.[1-5]

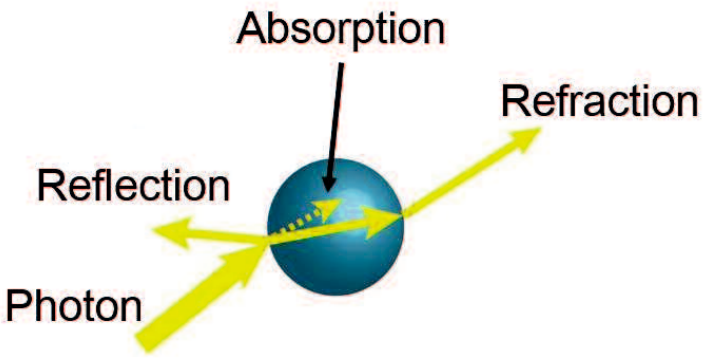

Figure 1-1. Optical phenomena when a photon impinge on a colloidal particle.

The existence of the radiation pressure of light was demonstrated by Lebedev[6] in 1901 and Nichols and Hull[7] in 1903 using a lamp and a torsion balance (Figure 1-2). Lebedev observed the radiation pressure of light qualitatively by irradiating light of an arc lamp to a thin metal plate attached to the balance using a fiber in vacuo. After that, Nichols and

Hull quantitatively estimated the radiation pressure of light by irradiating light of an arc lamp with approximately 1 mW to a mirror attached to the balance using a fiber. As a result, the radiation pressure of light was estimated to 7.01×10^{-10} N/cm^2 based on the equation of motion of the balance given by $x\frac{\partial^2\theta}{\partial t^2}+2\varepsilon\frac{\partial\theta}{\partial t}=-G\theta+L$, where x is the moment of inertia of the torsion balance, θ is the angle at which the torsion of the fiber balance the moment produced by the radiation pressure, ε is the damping constant, G is the moment of torsion of the fiber for $\theta=1$ radian, L is the moment of the radiation force. The radiation pressure of light emitted by an arc lamp was so small that the radiation pressure was not easily detected and any practical use seemed unfeasible.

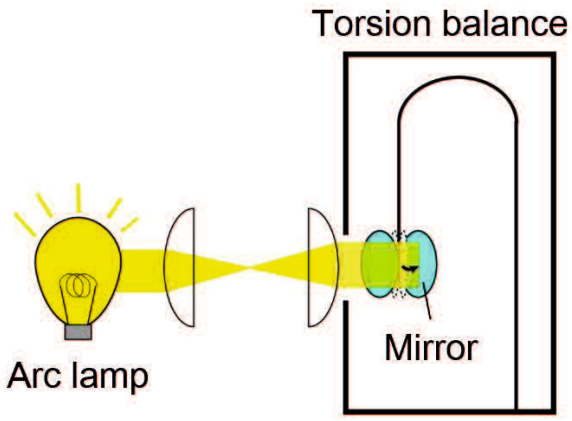

Figure 1-2. Experimental setup for observation of radiation pressure of light reported by Lebedev[6], Nichols and Hull[7].

The advent of a laser device at 1954 made it possible to practical use of the radiation pressure because of the intense power density of a laser beam. Since the 1960s, optical

manipulation of colloidal particles has been developed using the radiation pressure of a laser beam.[8-15] In 1970, stable optical trapping of 2.68 μm-sized latex spheres between a pair of counter-propagating laser beams was first demonstrated using radiation pressure of a continuous-wave argon laser with 128 mW.[16] In 1986, Ashkin et al. reported optical trapping of 10 μm-sized glass spheres by using a tightly focused laser beam of 100 mW.[17] Nowadays, the optical manipulation using a tightly focused laser beam is a popular technique for non-contact and non-invasive trapping, and for the transport of colloidal particles.

When a tightly focused laser beam is irradiated to colloidal particles, the particle is trapped at the focal point. At the time, a focused laser beam provides two types of forces as a laser radiation pressure on the trapped particle.[18-22] One is the scattering force and the other is the gradient force. The model for interpretation of these forces is proposed depending on the size of the trapped particle.

In the case of particles whose size is much larger than the wavelength of an incident laser beam, these forces are explained by geometrical optics.[18,20] Here, let us consider reflection and refraction of an incident laser beam at the interface between air and a transparent medium of higher refractive index than air, based on geometrical optics. Figure 1-3 shows schematic representation of radiation pressure exerted on a transparent

medium by reflection and refraction. When a laser beam impinges on the interface between two media with different refractive indices, part of it is reflected and the residual part is refracted. Although the reflection and the refraction occur simultaneously at the interface, for better interpretation of their phenomena, reflection is distinguished from refraction in Figure 1-3. Figure 1-3 (a) indicates the generation of radiation pressure owing to reflection of a laser beam. When an incident laser beam impinges on the interface at a given angle, θ, its propagation direction changes by reflection. As a result, the momentum of the incident laser beam, P_1, also changes into that of reflected laser beam, P_2. By the law of conservation of momentum, radiation pressure, F, is exerted vertically downward as a reaction force. Figure 1-3 (b) indicates the generation of radiation pressure owing to refraction of a laser beam. When an incident laser beam impinges on the interface at a given angle, its propagation direction changes by refraction. As a result, the momentum of the incident laser beam, P_1, also changes into that of the refracted laser beam, P_2. By the law of conservation of momentum, radiation pressure, F, is exerted vertically upward as a reaction force. The directions in which radiation pressure is exerted are different each other between reflection and refraction.

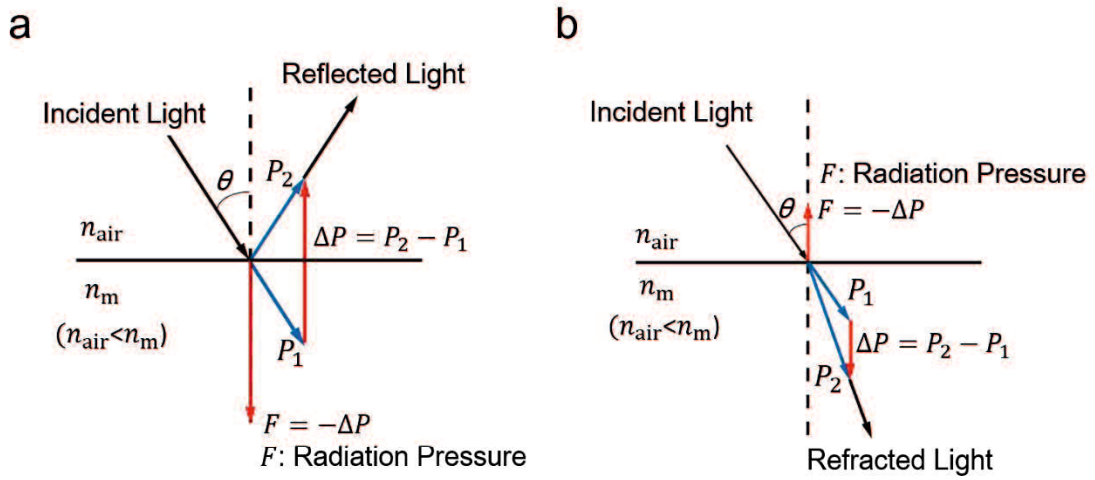

Figure 1-3. Schematic representation of generation of laser radiation pressure by (a) reflection and (b) refraction.

Based on the above explanation, let us consider the case that a tightly focused laser beam irradiates a spherical particle. Figure 1-4 shows forces exerted on a spherical particle of higher refractive index than its surrounding medium by irradiating a tightly focused laser beam. Figure 1-4 (a) shows a force on the spherical particle, which is induced by reflection of the focused laser beam. When the focused laser beam is reflected at the surface of the spherical particle (black arrows), radiation pressures (thin red arrows) are generated there. A total radiation pressure (thick red arrow), F, is exerted on the spherical particle. Thus, the reflection of the laser beam results in the force pushing the spherical particle toward the propagation direction of the incident laser beam. This force is called scattering force. Figure 1-4 (b) and (c) show forces on the spherical particle, which are induced by refraction of the focused laser beam. When the focused laser beam

is refracted through the spherical particle (black arrows), radiation pressures (thin red arrows) are generated there. A total radiation pressure (thick red arrows), F, is exerted on the spherical particle. Even when the spherical particle is located in the focal plane but not in the center (Figure 1-4 (b)) or not the focal plane but in the center of optical path after the focal point (Figure 1-4 (c)), the refraction of the laser beam results in forces attracting the spherical particle toward the focal point. This force is called gradient force. The scattering and gradient forces arise from reflection or refraction of a laser beam from the perspective of geometrical optics.

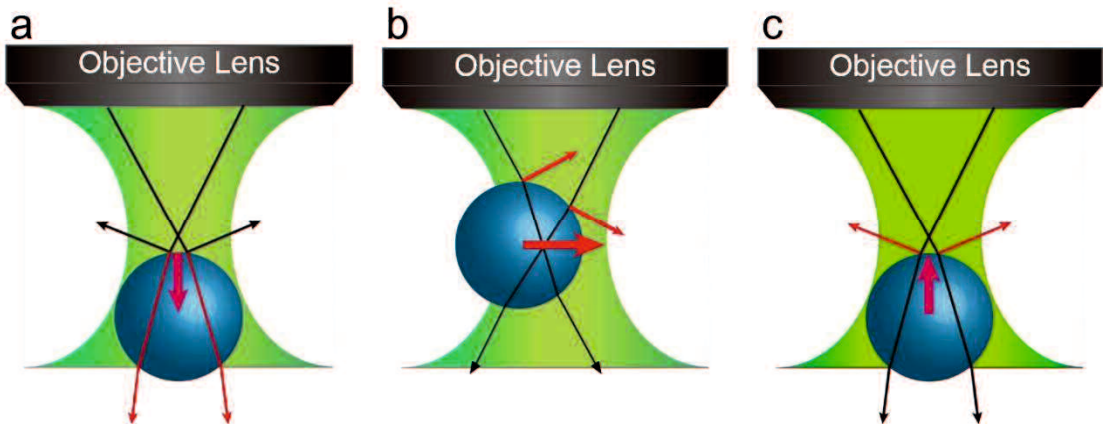

Figure 1-4. Schematic representation of the principle of optical trapping based on geometrical optics. For a spherical particle whose size is much larger than the wavelength of an incident laser beam, (a) a scattering force caused by reflection and (b), (c) gradient force caused by refraction are exerted. Black arrows indicate traces of a laser beam. Thin and thick red arrows indicate laser radiation pressures generated at the interface by reflection or refraction, and total laser radiation pressures, respectively.

In the case of particles whose size is much smaller than the wavelength of an incident laser beam, forces exerted on a particle are explained by the dipole approximation.[19,21,22] As for spherical particles in the Rayleigh scattering regime, polarization is induced on the particles by an incident laser beam. Therefore, the particle is treated as an induced small dipole confined in an optical field of the incident laser beam. For a dipole, the scattering force is exerted by momentum changes of the incident laser beam caused by light scattering. The gradient force is exerted by the Lorentz force acting on the induced dipole. The force exerted on a spherical particle is given by[22]

$$\begin{aligned}\mathbf{f}(\mathbf{r}) &= \mathbf{F}_{\mathrm{grad}}(\mathbf{r}) + \mathbf{F}_{\mathrm{scat}}(\mathbf{r}) \\ &= \frac{1}{2}\varepsilon_0\varepsilon_{\mathrm{m}}\mathrm{Re}[\alpha(\omega)]\nabla\langle \boldsymbol{E}(\mathbf{r},t)\rangle_{\mathrm{T}} + \frac{n_{\mathrm{m}}}{c}[C_{\mathrm{scat}} + C_{\mathrm{abs}}]\langle \boldsymbol{S}(\mathbf{r},t)\rangle_{\mathrm{T}}\end{aligned}$$

where ε_0 and ε_{m} are permittivity in the vacuum and the surrounding medium, $\alpha(\omega)$ is the polarizability of the spherical particle at a given wavelength, $\boldsymbol{E}(\mathbf{r},t)$ is the electric field vector, n_{m} is the refractive index of the surrounding medium, c is the speed of light, C_{scat} and C_{abs} are the scattering and absorption cross sections of the spherical particle. $\boldsymbol{S}(\mathbf{r},t)$ is the Poynting vector. The first term, $\mathbf{F}_{\mathrm{grad}}(\mathbf{r})$, is the gradient force and the second term, $\mathbf{F}_{\mathrm{scat}}(\mathbf{r})$, is the scattering force. The gradient force attracts a spherical particle toward the position with the highest laser intensity, namely, the focal point, while the scattering force pushes the spherical particle toward the propagation direction of the

incident laser beam. The equation indicates gradient force depends on the polarizability of the particle. The polarizability of the spherical particle is given by[22]

$$\alpha(\omega) = 4\pi a^3 \frac{\varepsilon_\mathrm{p} - \varepsilon_\mathrm{m}}{\varepsilon_\mathrm{p} + 2\varepsilon_\mathrm{m}}$$

where a is the radius of the particle, ε_p is the permittivity of the particle. Based on Mie scattering theory, the scattering and absorption cross sections of the spherical particle are given by[23]

$$C_\mathrm{scat} = \frac{n_\mathrm{m}^4 k_0^4}{6\pi} |\alpha(\omega)|^2$$

$$C_\mathrm{abs} = \frac{n_\mathrm{m} k_0}{\varepsilon_0} \mathrm{Im}[\alpha(\omega)]$$

where k_0 is the wavenumber in the vacuum. According to the equations, the wavelength of the incident laser beam, the refractive index, the size, and the polarizability of a target particle are important parameters for optical manipulation of particles in the Rayleigh scattering regime.

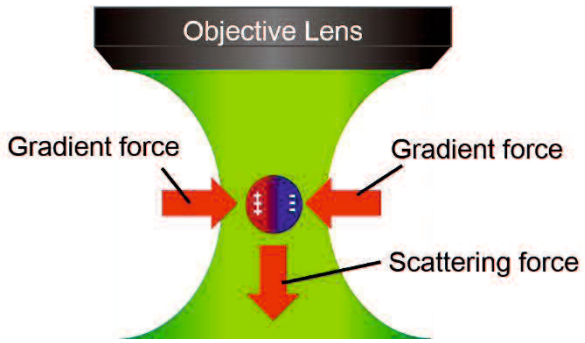

Figure 1-5. Schematic representation of optical trapping of a particle whose size is much smaller than the wavelength of an incident laser beam.

To date, optical manipulation of spherical colloidal particles have been applied in various fields since Ashkin demonstrated optical trapping of glass spheres by a tightly focused laser beam in 1986.[17] Ashkin et al. reported optical trapping of an individual tobacco mosaic virus and an *Escherichia coli* bacterium in 1987.[24] Block et al. observed the movement of a kinesin molecule on a microtubule through the motion of an optically trapped microscopic silica bead immobilized kinesin molecules.[25] Finer et al. measured force and displacement that resulted from the interaction of a single myosin molecule with a single suspended actin filament in 1994.[26] In 2006, Li et al. reported optical trapping of fluorophore-labeled LP2-IgG antibodies.[27] Tsuboi et al. reported optical trapping of microparticle composed of amino acids[28] and myoglobins[29] in 2010 and 2013, respectively. For physical and chemical applications, in 1991, Misawa et al. reported three-dimensional optical trapping and laser ablation of a poly(methylmethacrylate) latex particle.[30] In 1994, Svoboda and Block reported optical trapping of gold nanoparticles.[31] In 1999, Won et al. reported optical manipulation of polystyrene particles and its photothermal fixation.[32] In 2004, King et al. reported optical trapping of aerosol droplets and their Raman spectroscopy.[33] In 2005, Murazawa et al. reported optical manipulation of liquid crystal droplets and molecular alignment change inside the droplets.[34] In 2006, Inaba et al. reported optical manipulation of CuCl nanoparticles and the transportation

depending on their size.[35] In 2011, Ohlinger et al. reported three-dimensional optical trapping of plasmonically coupled silver nanoparticles.[36]

1-1-2. Optical Manipulation of One-dimensional Materials and Their Orientation

Recently, optical manipulation of colloidal particles has been extended from spherical particles to one-dimensional (1D) rod-like materials. The 1D materials are trapped at a focal point as is the trapping of the spherical particles described in section 1-1-1. In addition, for the 1D materials, the laser radiation pressure contributes to their orientation manipulation. When irradiating a tightly focused beam to 1D materials, the materials orient their long-axis parallel to the propagation direction of the incident laser beam so as to minimize the scattering force at the focal point and they are trapped by the gradient force, as shown in Figure 1-6. This type of orientation manipulation is commonly seen for elongated objects such as 1D rod-like materials. For example, carbon nanotubes,[37-40] polymer nanofibers,[41] metal nanowires[42,43] and semiconductor nanowires[44-49] have been oriented in the similar manner as shown in Figure 1-6. Thus, radiation pressure can be utilized for orientation manipulation of uniaxial anisotropic materials. It should be noted here that 1D material have large shape anisotropy. Typically, the size of long-axis direction is in the geometrical optics regime, while the short-axis direction is in the Rayleigh scattering regime. Therefore, theoretical consideration of optical trapping of anisotropic materials such as 1D materials is not fully understood yet.

Figure 1-6. Schematic representation of an optically trapped one-dimensional rod-like material by a tightly focused laser beam.

1-2. Objective and Outline of This Work

In the optical manipulation of anisotropic materials, target materials are still limited to 1D materials so far and two-dimensional (2D) plate-like materials are not manipulated yet. In this study, trapping and orientation manipulation of colloidal 2D plate-like materials have been attempted using a tightly focused laser beam.

In contrast to 1D materials, the orientation of 2D materials is completely determined by two axes orthogonal in-plane because of their biaxial shape. Polarization dependence of radiation pressure exerted on an anisotropic object has theoretically been considered. In 2009, Ajiki et al. reported that the magnitude of the scattering and gradient forces exerted on a single walled carbon nanotube was dependent on the polarization.[50] As shown in Figure 1-7, They set *x* and *y* coordinates in the circumference and axial direction of the carbon nanotube, respectively. The propagation direction of the polarized laser beam is along to the *z*-axis. They estimated the forces for each of two polarization states. One polarization is parallel and the other polarization is perpendicular to the long-axis of the carbon nanotube. According to them, the potential due to gradient force for parallel polarization is about 40 times larger than that for perpendicular polarization. Thus, the magnitude of the gradient forces exerted on anisotropic materials is expected to depend on the polarization direction of the incident laser beam. Therefore, it could be possible to

realize biaxial orientation when a 2D material is trapped using a polarized laser beam.

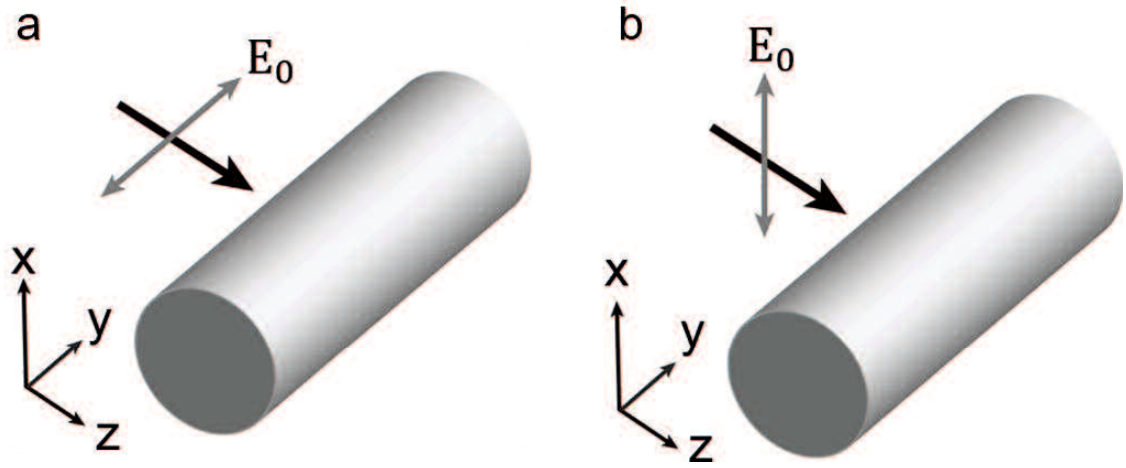

Figure 1-7. Schematic illustration of a laser irradiation with (a) parallel or (b) perpendicular oscillating electric field to the long-axis to a one-dimensional material.

Namely, when a 2D material is trapped to orient one of their axis parallel to the propagation direction of an incident laser beam as is the case of 1D materials, the other axis could be controlled by polarization of the incident laser beam. In fact, when an alternating current electric field is applied to nanosheets in colloidal state, they are aligned parallel to the applied electric field.[51-54] About the general description of nanosheet, see Appendix A. Therefore, nanosheets are expected to be aligned along the polarization direction of an optical electric field. If the orientation of nanosheets are controlled by light, the local and precise orientation control of 2D materials should be realized. Thus, in this study, trapping and orientation manipulation of colloidal 2D materials using a radiation

pressure of a tightly focused laser beam have been attempted.

The sample preparation and experimental setup were explained in Chapter 2. Niobate nanosheets were employed as a model of a 2D plate-like material because their orientation by external forces has been well investigated. A polarized continuous-wave laser beam emitting at 532 nm was focused into the sample using an objective lens at room temperature. Orientation behavior of niobate nanosheets under laser irradiation was observed with polarized and bright-field optical microscopes.

In Chapter 3, trapping and orientation manipulation of randomly dispersed colloidal nanosheets was demonstrated. When a linearly polarized laser beam was irradiated to an isotropic nanosheet colloid, the nanosheets were trapped at the focal point and oriented their in-plane direction parallel to the propagation direction of the incident laser beam. In addition, the trapped nanosheet was found to align along the polarization direction of the incident laser beam and rotated with the rotation of the polarization direction. When a circularly polarized laser beam was irradiated to the isotropic nanosheet colloid, the trapped nanosheet was found to rotate continuously.

In Chapter 4, orientation manipulation of nanosheets in colloid which exhibit lyotropic liquid crystallinity was demonstrated. Nanosheets in a colloid are known to exhibit liquid crystallinity when the concentration, the size of the nanosheet and so forth

have been optimized (details are in Appendix B).[55] The liquid crystalline nanosheets can change their orientation to construct homogenous orientation in the same manner in the entire sample in response to an external field such as a shear force and an electric field.[51-54] In this study, a local and on-demand orientation switching has been realized for the first time by utilizing radiation pressure. When a linearly polarized laser beam irradiated a niobate nanosheet liquid crystal, a local but giant hierarchical structure consisted of two domains was generated. One domain was found close to the focal point. The size of the domain was 15 μm, which was 50 times larger than that of the focal point. In this domain, nanosheets oriented their in-plane direction parallel to the propagation direction and the polarization direction of the incident laser beam. This behavior was essentially the same as the orientation manipulation of a colloidal nanosheet in an isotropic phase. The other domain was found at the periphery of the domain close to the focal point. The size of the domain was more than 110 μm, which was 370 times larger than that of the focal point. In the domain, nanosheets which oriented their in-plane direction parallel to the propagation direction of the incident laser beam formed a tree-ring-like texture. Thus, nanosheets were found to form a large hierarchical structure owing to a large excluded volume characteristic to liquid crystalline nanosheets.

References

1. A. Ashkin and J. M. Dziedzic, Appl. Phys. Lett. **1971**, *19*, 283-285.
2. J. H. Poynting, *Phil. Trans. R. Soc. Lond* **1884**, *175*, 343-361.
3. Y. Harada and T. Asakura, *Pure Appl. Opt.* **1998**, *7*, 1001-1012.
4. T. Iida and H. Ishihara, *Phys. Rev. B* **2008**, *77*, 245319.
5. T. Kudo and H. Ishihara, *Phys. Chem. Chem. Phys.* **2013**, *15*, 14595-14610.
6. P. Lebedev, *Ann. Phys.* **1901**, *311*, 433-458.
7. E. F. Nichols and G. F. Hull, *Phys. Rev.* **1903**, *17*, 26-50.
8. A. Ashkin, *Phys. Rev. Lett.* **1970**, *24*, 156-159.
9. A. Ashkin, *Science* **1980**, *210*, 1081-1088.
10. A. Ashkin, J. M. Dziedzic, J. E. Bjorkholm and S. Chu, *Opt. Lett.* **1986**, *11*, 288-290.
11. D. G. Grier, *Nature* **2003**, *424*, 810-816.
12. K. Dholakia, P. Reece and M. Gu, *Chem. Soc. Rev.* **2008**, *37*, 42-55.
13. S. E. S. Spesyvtseva and K. Dholakia, *ACS Photonics* **2016**, *3*, 719-736.
14. K. Dholakia and T. Čižmár, *Nature Photon.* **2011**, *5*, 335-342.
15. M. Padgett and R. Bowman, *Nature Photon.* **2011**, *5*, 343-348.
16. A. Ashkin, *Phys. Rev. Lett.* **1970**, *24*, 156-159.
17. A. Ashkin, J. M. Dziedzic, J. E. Bjorkholm and S. Chu, *Opt. Lett.* **1986**, *11*, 288-290.
18. A. Ashkin, *Biophys. J.* **1992**, *61*, 569-582.
19. Y. Harada and T. Asakura, *Opt. Commun.* **1996**, *124*, 529-541.
20. Y. -R. Chang, L. Hsu and S. Chi, *Appl. Opt.* **2006**, *45*, 3885-3892.
21. N. Malagnino, G. Pesce, A. Sasso and E. Arimondo, *Opt. Commun.* **2002**, *214*, 15-24.
22. M. Dienerowitz, M. Mazilu and K. Dholakia, *J. Nanophoton.* **2008**, *2*, 021875.
23. G. Mie, *Ann. d. Physik*, **1908**, *4*, 378-445.
24. A. Ashkin and J. M. Dziedzic, *Science* **1987**, *235*, 1517-1520.
25. S. M. Block, L. S. B. Goldstein and B. J. Schnapp, *Nature* **1990**, *348*, 348-352.
26. J. T. Finer, R. M. Simmons and J. A. Spudich, *Nature* **1994**, *368*, 113-119.
27. H. Li, D. Zhou, H. Browne and D. Klenerman, *J. Am. Chem. Soc.* **2006**, *128*, 5711-5717.
28. Y. Tsuboi, T. Shoji and N. Kitamura, *J. Phys. Chem. C* **2010**, *114*, 5589-5593.
29. T. Shoji, N. Kitamura and Y. Tsuboi, *J. Phys. Chem. C* **2013**, *117*, 10691-10697.
30. H. Misawa, M. Koshioka, K. Sasaki, N. Kitamura and H. Masuhara, *J. Appl. Phys.* **1991**, *70*, 3829-3836.
31. K. Svoboda and S. M. Block, *Opt. Lett.* **1994**, *19*, 930-932.
32. J. Won, T. Inaba, H. Masuhara, H. Fujiwara, K. Sasaki, S. Miyawaki and S. Sato,

Appl. Phys. Lett. **1999**, *75*, 1506.
33. M. D. King, K. C. Thompson and A. D. Ward, *J. Am. Chem. Soc.* **2004**, *126*, 16710-16711.
34. N. Murazawa, S. Juodkazis, S. Matsuo and H. Misawa, *Small* **2005**, *1*, 656-661.
35. K. Inaba, K. Imaizumi, K. Katayama, M. Ichiyama, A. Ashida, T. Iida, H. Ishihara and T. Itoh, *Phys. Stat. sol.* **2006**, *14*, 3829-3833.
36. A. Ohlinger, S. Nedev, A. A. Lutich and J. Feldmann, *Nano Lett.* **2011**, *11*, 1770-1774.
37. S. Tan, H. A. Lopez, C. W. Cai and Y. Zhang, *Nano Lett.* **2004**, *4*, 1415-1419.
38. O. M. Maragò, P. H. Jones, F. Bonaccorso, V. Scardaci, P. G. Gucciardi, A. G. Rozhin and A. C. Ferrari, *Nano Lett.* **2008**, *8*, 3211-3216.
39. P. J. Pauzauskie, A. Jamshidi, J. K. Valley, J. H. Satcher and M. C. Wu, *Appl. Phys. Lett.* **2009**, *95*, 113104.
40. M. -Y. Wu, D. -X. Ling, L. Ling, W. Li and Y. -Y. Li, *Sci. Rep.* **2017**, *7*, 42930.
41. A. A. R. Neves, A. Camposeo, S. Pagliara, R. Saija, F. Borghese, P. Denti, M. A. Iatì, R. Cingolani, O. M. Maragò and D. Pisignano, *Opt. Express* **2010**, *18*, 822-830.
42. L. Tong, V. D. Milijković and M. Käll, *Nano Lett.* **2010**, *10*, 268-273.
43. Z. Yan, J. E. Jureller, J. Sweet, M. J. Guffey, M. Pelton and N. F. Scherer, *Nano Lett.* **2012**, *12*, 5155-5161.
44. S. -W. Lee, G. Jo, T. Lee and Y. -G. Lee, *Opt. Express* **2009**, *17*, 17491-17501.
45. P. J. Reece, S. Paiman, O. Abudul-Nabi, Q. Gao, M. Gal, H. H. Tan and C. Jagadish, *Appl. Phys. Lett.* **2009**, *95*, 101109.
46. P. J. Reece, W. J. Toe, F. Wang, S. Paiman, Q. Gao, H. H. Tan and C. Jagadish, *Nano Lett.* **2011**, *11*, 2375-2381.
47. F. Dutto, C. Raillon, K. Schenk and A. Radenovic, *Nano Lett.* **2011**, *11*, 2517-2521.
48. A. Irrera, P. Artoni, R. Saija, P. G. Gucciardi, M. A. Iatì, F. Borghese, P. Denti, F. Iacona, F. Priolo and O. M. Maragò, *Nano Lett.* **2011**, *11*, 4879-4884.
49. F. Wang, W. J. Toe, W. M. Lee, D. McGloin, Q. Gao, H. H. Tan, C. Jagadish and P. J. Reece, *Nano Lett.* **2013**, *13*, 1185-1191.
50. H. Ajiki, T. Iida, T. Ishikawa, S. Uryu and H. Ishihara, *Phys. Rev. B* **2009**, *80*, 115437.
51. N. Miyamoto and T. Nakato, *J. Phys. Chem. B* **2004**, *108*, 6152-6159.
52. T. Nakato, K. Nakamura, Y. Shimada, Y. Shido, T. Houryu, Y. Iimura and H. Miyata, *J. Phys. Chem. C* **2011**, *115*, 8934-8939.
53. T. Nakato, Y. Nono, E. Mouri and M. Nakata, *Phys. Chem. Chem. Phys.* **2014**, *16*, 955-962.
54. T. Nakato, Y. Nono and E. Mouri, *Colloidal Surf., A* **2017**, *522*, 373-381.

55. T. Nakato and N. Miyamoto, *Materials* **2009**, *2*, 1734-1761.

Chapter 2. Samples and Experimental Setup

2-1. Preparation of Colloidal Two-dimensional Materials

As a model of colloidal 2D material, a niobate nanosheet colloid was employed in this study. This is because their orientation control by an external field such as a shear force[1] and an electric field[2] has been established. The niobate nanosheet colloid was prepared by exfoliation of layered $K_4Nb_6O_{17}$. A high concentration niobate nanosheet colloid was provided by Prof. Teruyuki Nakato at Kyusyu Institute of Technology. The detailed method for preparation of the niobate nanosheet colloid can be referred in his publications.[1,2] The sample was prepared by diluting the provided nanosheet colloid with ultrapure water to 0.05 g/L and 5 g/L of the nanosheet concentration. The lateral lengths of the provided nanosheets had a size distribution that obeyed a long-normal distribution to yield an average size of 1.6 μm. The thickness of the employed niobate nanosheet was 1.8 nm. The samples that were prepared at concentrations of 0.05 g/L and 5 g/L exhibited an isotropic phase, and a biphasic mixture of isotropic and liquid crystalline phases at room temperature, respectively.

2-2. Experimental Setup for Optical Microscope Observation under Laser Irradiation

Figure 2-1 and Figure 2-2 show schematic representation and a photograph of the experimental setup, respectively. The sample was injected into 100-μm-thick thin-layer glass cell (see inset of Figure 2-1). The cell was set on the stage of an inverted microscope (IX70, Olympus). A linearly polarized continuous-wave laser beam that emits at 532 nm (Millennia Pro, Spectra Physics) was focused at the center of the cell (50 μm from the cell-sample interface) using an objective lens (60×, numerical aperture = 1.20) at room temperature. The laser power was set to 20 mW after the objective lens unless otherwise noted. The beam diameter was adjusted to the pupil diameter of the objective lens by using a beam expander. The polarization direction of the linearly polarized laser beam was controlled by rotating a half-wave plate. The circularly polarized laser beam was generated by inserting a quarter-wave plate instead of the half-wave plate.

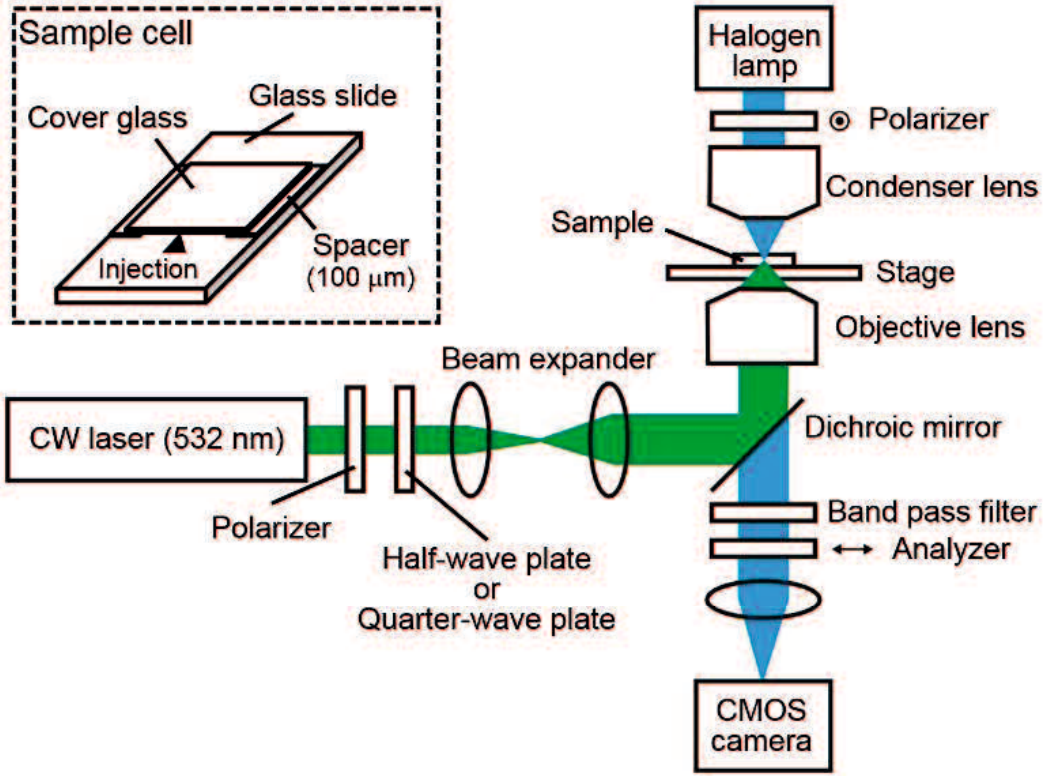

Figure 2-1. Schematic representation of the experimental setup to observe niobate nanosheets under laser irradiation.

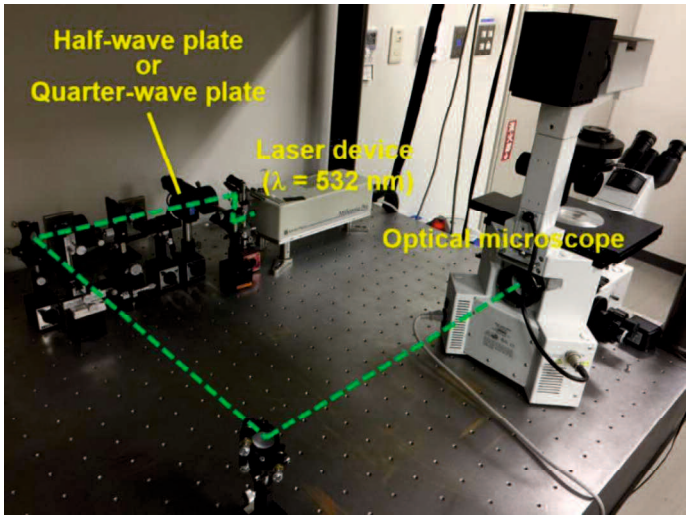

Figure 2-2. Photograph of the experimental setup. The green broken line indicates the beam path of the laser.

For polarized optical microscope observation upon irradiation with a laser beam, the sample was illuminated by a halogen lamp, and the image was monitored with a digital CMOS camera (ORCA-Flash 4.0 V3, Hamamatsu Photonics). A pair of crossed polarizers (polarizer and analyzer) was inserted out of the beam pass of the laser beam. For bright-field optical microscope observation, the same experimental setup without a polarizer and an analyzer was used. The incident laser beam was blocked completely by a dichroic mirror and a band pass filter that were inserted before the camera. A spatial resolutions in our setup was estimated to 330 nm.[3] The value was almost the same size as the diffraction limits.

References

1. N. Miyamoto and T. Nakato, *J. Phys. Chem. B* **2004**, *108*, 6152-6159.
2. T. Nakato, Y. Nono, E. Mouri and M. Nakata, *Phys. Chem. Chem. Phys.* **2014**, *16*, 955-962.
3. H. H. Hopkins and P. M. Barham, *Proc. Phys. Soc. London* **1950**, *63*, 737-744.

Chapter 3. Optical Trapping and Orientation Manipulation of Randomly Dispersed Two-dimensional Materials

In this Chapter, a laser beam was irradiated to a niobate nanosheet colloid with a concentration of 0.05 g/L, in which the nanosheet is randomly dispersed.

3-1. Trapping of a Randomly Dispersed Nanosheet by a Linearly Polarized Laser Beam

The optical microscope images of a nanosheet colloid before and after irradiation with a linearly polarized laser beam are shown in Figure 3-1. An object that looks like a line or rod shape with a length of 1-10 μm was found to be trapped at the focal point when the laser beam was irradiated. Hereafter, these are referred as “line-shaped object”. Before laser irradiation, many line-shaped objects were observed within the microscope field as shown in Figure 3-1 (a). The line-shaped objects were moved and/or appeared and disappeared owing to the focusing and defocusing by three-dimensional Brownian motion. This is because the depth of field for our observation was 420 nm, which is only 0.42% of the thickness of the cell. When a nanosheet orients its in-plane direction parallel to the propagation direction of an incident laser beam, the nanosheet should be observed as a

line. Therefore, the line-shaped objects were attributed to nanosheets which oriented their in-plane direction parallel to the propagation direction of the incident laser beam. Figure 3-1 (b) shows the image after 15 s of continuous laser irradiation. No apparent change was observed at the focal point and the Brownian motion seen over the entire microscope field was continuously observed. After 30 s of continuous laser irradiation, a line-shaped object appeared near the focal point (Figure 3-1 (c)). This line-shaped object was moved toward the focal point and then was completely trapped at the focal point after 34 s of continuous laser irradiation (Figure 3-1 (d)) and no longer disappeared during laser irradiation. The trapped object aligned along the polarization direction of the incident laser beam. There was a variation of 20 s to 34 s in the time required for trapping of the line-shaped object after starting the laser irradiation.

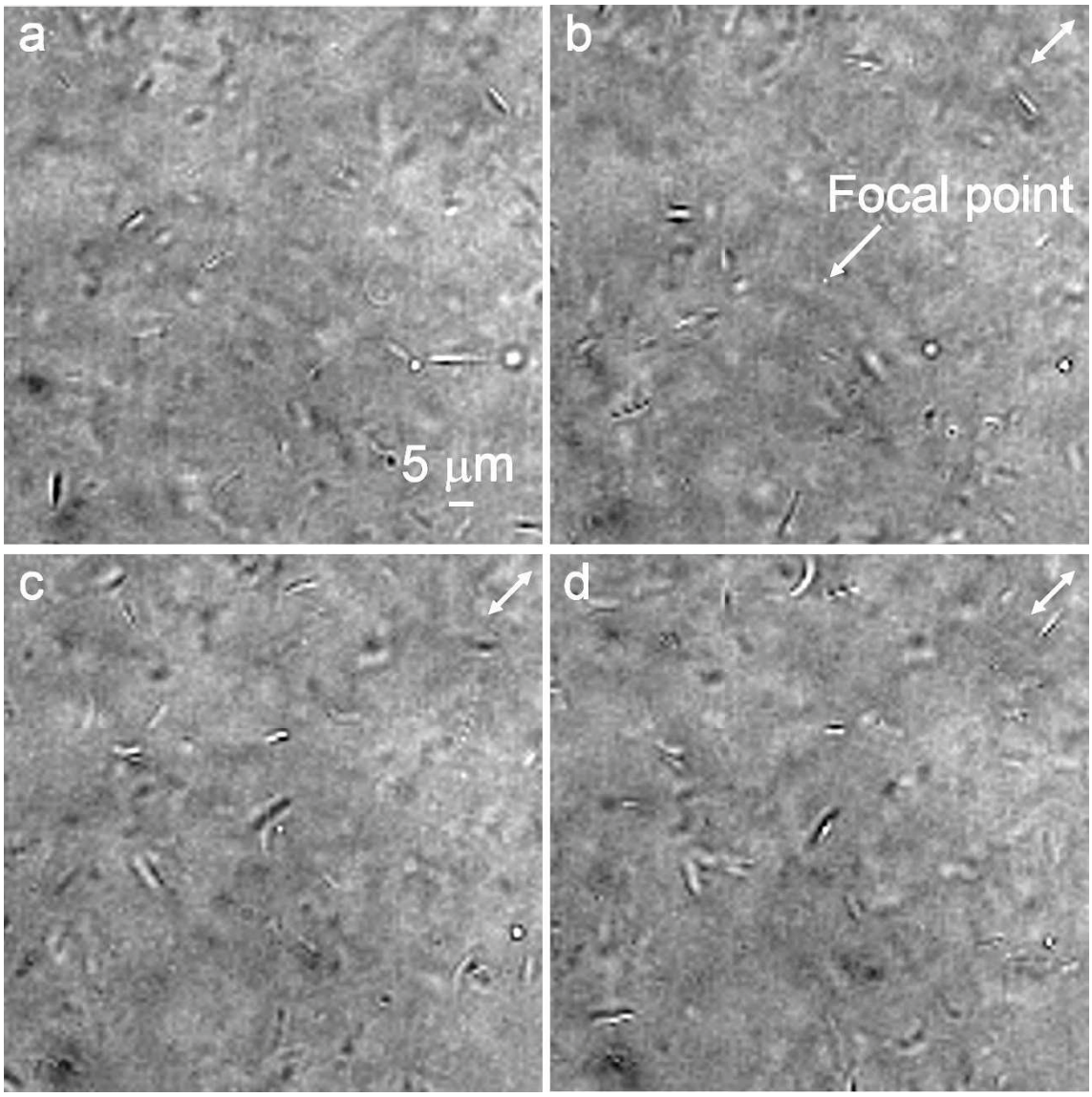

Figure 3-1. Bright-field optical microscope images of a niobate nanosheet colloid (a) before laser irradiation and after (b) 15 s, (c) 30 s, and (d) 34 s of continuous laser irradiation with a linearly polarized laser beam. The very small white point shown in (b) represents the focal spot with a diameter of 0.3 μm. The white double arrows indicate the polarization direction.

The orientation behavior of a nanosheet by laser irradiation can be considered as an analogy of the orientation manipulation of 1D materials. In general, a focused laser beam provides two types of forces as a radiation pressure on a particle[1-5] as described in Chapter

1. One is a scattering force which is applied toward the propagation direction of the incident laser beam to the object. The other is a gradient force which is applied perpendicular to the propagation direction of the incident laser beam. As described in Chapter 1, 1D materials orient their long-axis parallel to the propagation direction of an incident laser beam to minimize the scattering force and then they are trapped by the gradient force when a focused laser beam is used to irradiate them.[6] In the case of a niobate nanosheet, the aspect ratio of the lateral length to its thickness is approximately 1:1000. Therefore, the forces being applied in the direction perpendicular to the surface of the nanosheet are dominant and the force being applied in the direction parallel to the surface of the nanosheet is negligible. As is the case for 1D materials, a nanosheet was thought to be oriented with its in-plane direction parallel to the propagation direction of an incident laser beam so as to minimize the scattering force.

The appearance of a line-shaped object at the focal point can be explained by the following mechanism. The thickness of the sample cell, 100 μm, was approximately 250 times larger than the depth of field. As described above, the nanosheets in the colloids randomly move by three-dimensional Brownian motion. A nanosheet coming into the optical path, including the defocus field, should be attracted to the focal point by a scattering and/or a gradient force and then the object will appear in the obtained

microscope image. Continuous laser irradiation of approximately 30 s was required until the line-shaped object appeared in Figure 3-1 (c). The reason why such a long time was required is considered to arise from the low concentration of the nanosheet colloid used in this study. Hence, approximately 30 s was required for a nanosheet to come into the optical path. Actually, it was confirmed that the time required for trapping a line-shaped object became longer when the concentration was further diluted.

3-2. Manipulation of the Trapped Nanosheet by Rotating the Polarization Direction of the Irradiated Laser Beam

Figure 3-2 shows that the trapped nanosheet at the focal point was rotated following rotation of the polarization direction of the incident laser beam. Figure 3-2 (a) shows a trapped nanosheet by irradiation of a laser beam with a polarization direction of 45° with respect to the viewing direction. When the polarization direction was rotated clockwise by 45°, the trapped nanosheet was also rotated clockwise by 45° (Figure 3-2 (b)). When the polarization direction was sequentially rotated by a further 45°, the trapped naonsheet was rotated following the rotation of the polarization direction (Figure 3-2 (c) and Figure 3-2 (d)). This fact indicates that the alignment was determined by the optical electric field of the linearly polarized incident laser beam. The rotation of the trapped line-shaped object followed that of the polarization direction in real-time until the upper limit of the rotation speed of the employed experimental setup, which was 0.4 π rad/s.

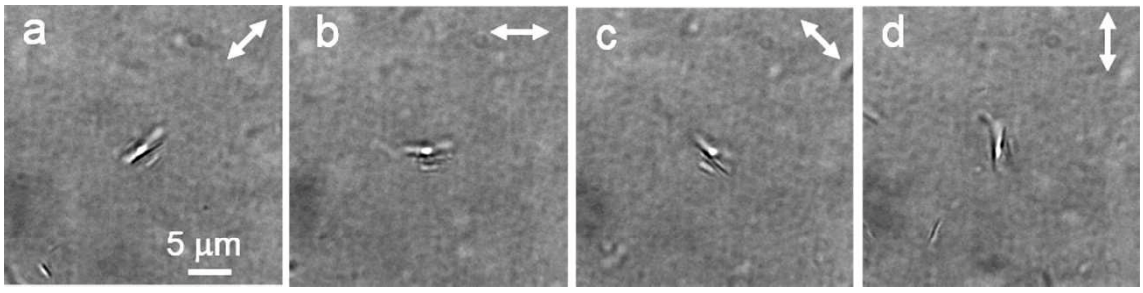

Figure 3-2. Bright-field optical microscope images of a niobate nanosheet colloid under rotation of the polarization direction of the incident laser beam. The white double arrows indicate the polarization direction, respectively.

3-3. Optical Trapping of Nanosheets by a Circularly Polarized Laser Beam

As described in section 3-2, the nanosheet was trapped at the focal point and rotated with rotation of the linearly polarized laser beam. Therefore, when a circularly polarized laser beam is irradiated to a nanosheet colloid, the trapped nanosheet is expected to rotate continuously. This is because a circularly polarized laser beam possesses the spin angular momentum.[7,8] Figure 3-3 (a) and 3-3 (g) show the bright-field optical microscope images of a nanosheet colloid before laser irradiation. When the left-handed circularly polarized laser beam was irradiated, a nanosheet was trapped at the focal point after 34 s of continuous laser irradiation as shown in Figure 3-3 (b), as is the case of the optical trapping of a nanosheet by laser irradiation with linear polarization. After 36 s of continuous laser irradiation, the trapped nanosheet began continuous rotation counterclockwise (Figure 3-3 (c)-(f)). On the other hand, even when the right-handed circularly polarized laser beam was irradiated, a nanosheet was also trapped after 34 s of continuous laser irradiation (Figure 3-3 (h)). The clockwise continuous rotation of the trapped nanosheet started after 39 s of continuous laser irradiation (Figure 3-3 (i)-(l)). Thus, rotation directions of the trapped nanosheet were switched by controlling the direction of the circularly polarized laser beam.

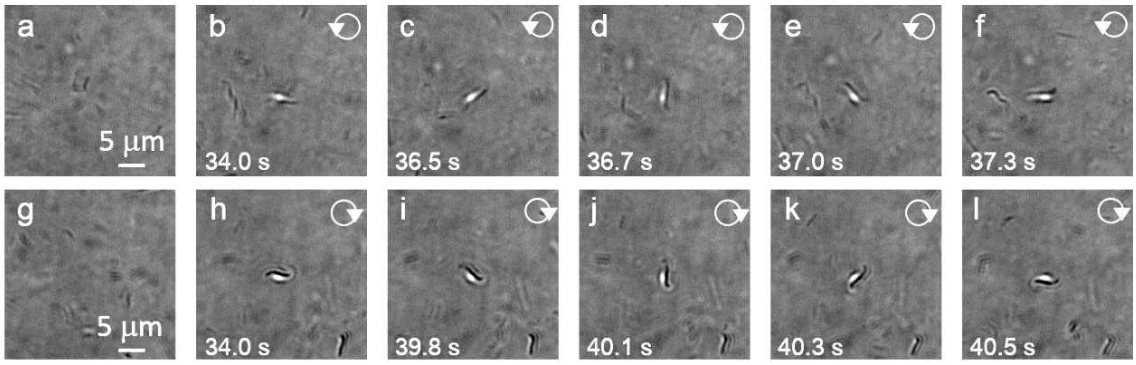

Figure 3-3. Optical microscope images of a niobate nanosheet colloid (a, g) before laser irradiation, and after irradiation of a left-handed circularly polarized laser beam (b-f) or a right-handed circularly polarized laser beam (h-l).

The rotational speed of the trapped nanosheet depended on the laser power of the irradiated circularly polarized laser beam, or viscosity of the sample. Figure 3-4 shows the laser power dependence of the rotational speed of the trapped nanosheet. The nanosheet was not trapped when the irradiated laser power was lower than 10 mW. On the other hand, when the irradiated laser power was more than 10 mW, it was trapped at the focal point and then rotated. In other words, the threshold of laser power to trap a nanosheet was 10 mW. The rotational speed at the laser power of 10 mW, 0.31 π rad s^{-1}, was much slower than that of the electric field vector of the irradiated circularly polarized laser beam. The rotational speed of the trapped nanosheet became faster as the irradiated laser power increased up to 50 mW. The result was consistent with the general relationship between rotational speed of a trapped object and irradiated laser power in optical manipulation using a circularly polarized laser beam.[7,9] However, when the

irradiated laser power was more than 50 mW, the rotational speed was not proportional to the irradiated laser power, and the increment became small. The possible reason is the rotation of the trapped nanosheet did not overcome viscosity of water.

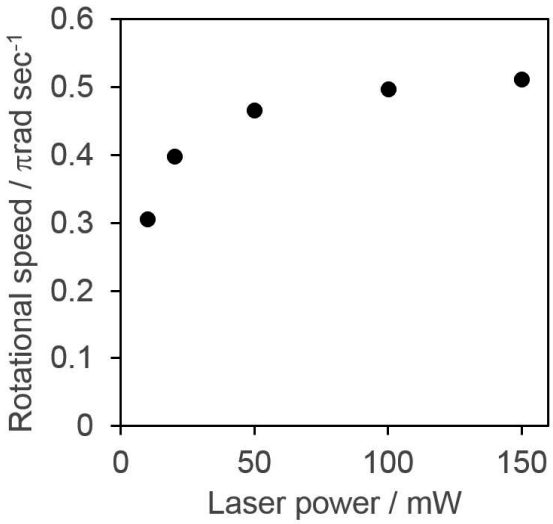

Figure 3-4. Rotational speed of the nanosheet trapped at the focal point for various laser powers of the irradiated circularly polarized laser beam.

Figure 3-5 shows the viscosity dependence of the rotational speed of the trapped nanosheet when the circularly polarized laser beam of 20 mW was irradiated. The viscosity of the sample was controlled by adding polyethylene glycol (19.9 mPa·s at 20ºC), which has higher viscosity than water (1.00 mPa·s at 20ºC), to the niobate nanosheet colloid. In Figure 3-5, the rotational speed was plotted against volume ratio of ethylene glycol in the viscosity-controlled sample. The rotational speed became slower

as the volume ratio of ethylene glycol was increased, namely the viscosity of the sample became higher. Because the nanosheet trapped at the focal point orients its in-plane direction parallel to the propagation direction of the irradiated laser beam, the surface of the nanosheet will receive large resistance from the surrounding medium, namely water, when the trapped nanosheet was rotated. Because the resistance becomes large as the viscosity increases, it could be thought that the rotational speed of the trapped nanosheet became slower as the viscosity of the sample became high.

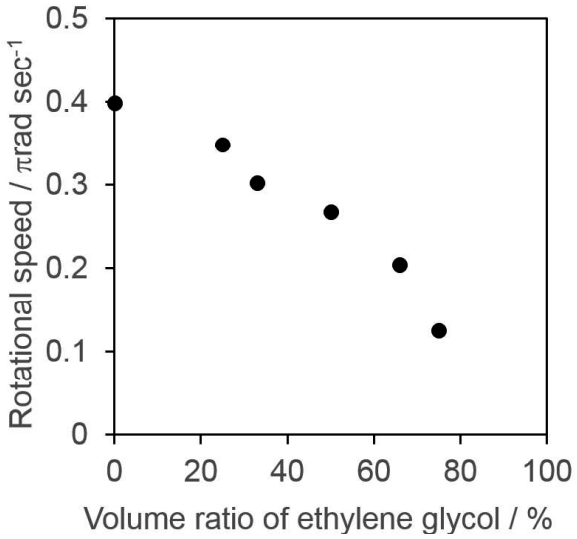

Figure 3-5. Rotational speed of the nanosheet trapped at the focal point. Horizontal axis shows the volume ratio of ethylene glycol in the ethylene glycol/water mixture used for the dispersion media of nanosheet.

3-4. On-demand Optical Manipulation by On-off Switching of Laser Irradiation

The nanosheet trapped at the focal point was gradually released when the laser irradiation was ceased. Figure 3-6 (a) shows the image just after the laser irradiation was ceased. The nanosheet trapped at the focal point began the Brownian motion again. The nanosheet was then gradually diffused and became blurred as shown in Figure 3-6 (b) and 3-6 (c). At 15 s after the laser irradiation ceased (Figure 3-6 (d)), the image was essentially the same as that before laser irradiation (see Figure 3-1 (a)).

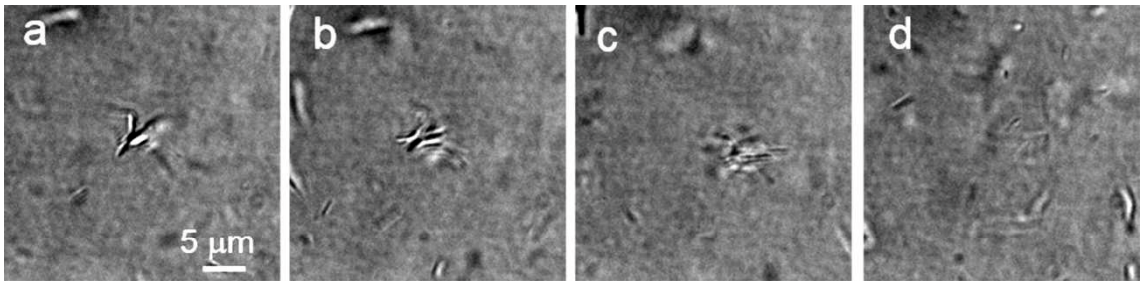

Figure 3-6. Bright-field optical microscope images of a niobate nanosheet colloid at (a) 0 s, (b) 2 s, (c) 10 s, and (d) 15 s after laser irradiation ceased.

The nanosheet was repeatedly trapped at the focal point by on-off switching of the laser irradiation. As shown in Figure 3-7 (a), upon irradiation with the laser beam at 15 s after the laser irradiation ceased, the nanosheet was re-trapped at the focal point after approximately 30 s of continuous laser irradiation. After the laser irradiation was ceased again, the re-trapped nanosheet diffused and was no longer observed as shown in Figure

3-7 (b). The re-trapping and releasing was repeated by further on-off switching cycles of the laser irradiation (Figure 3-7 (c) and Figure 3-7 (d)). Thus, on-demand optical manipulation was demonstrated by on-off switching of laser irradiation.

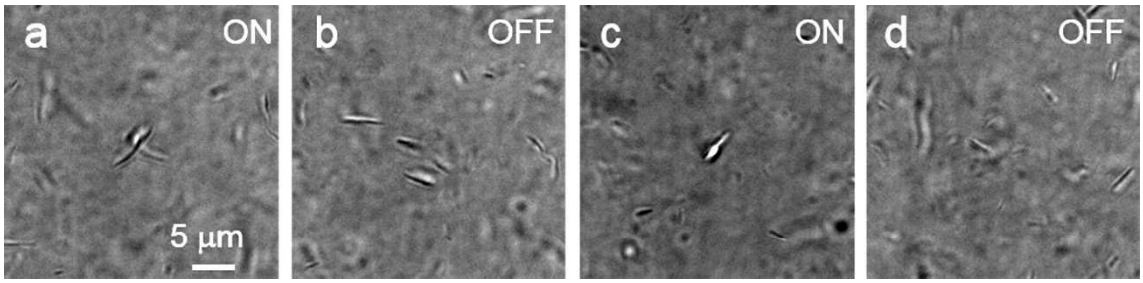

Figure 3-7. Bright-field optical microscope images of a re-trapped and released line-shaped object by on-off switching of the laser irradiation.

3-5. Conclusion

In this Chapter, first observation of optical trapping and orientation manipulation of a 2D material, niobate nanosheet, has been described. When a linearly polarized laser beam was irradiated to randomly dispersed nanosheets, a nanosheet was trapped at the focal point to orient its in-plane direction parallel to the propagation direction of the incident laser beam, as is the case of 1D materials. In addition, the trapped nanosheet aligned along the polarization direction of the incident laser beam and rotated with the rotation of the polarization direction. This is attributed to the biaxial shape characteristic to a nanosheet. It is concluded that the alignment of the trapped nanosheet was precisely controllable by a linearly polarized laser beam.

When a circularly polarized laser beam was irradiated, the trapped nanosheet was rotated continuously by the spin angular momentum of the circularly polarized laser beam. The rotation direction of the trapped nanosheet was switchable by controlling the direction of the circularly polarized laser beam. In addition, the rotation speed of the trapped nanosheet depended on the power of the irradiated circularly polarized laser beam or viscosity of the sample. As the irradiated laser power increased, or the viscosity of the sample decreased, the rotational speed of the trapped nanosheet tended to be faster.

References

1. A. Ashkin, *Biophys. J.* **1992**, *61*, 569-582.
2. Y. Harada and T. Asakura, *Opt. Commun.* **1996**, *124*, 529-541.
3. Y. -R. Chang, L. Hsu and S. Chi, *Appl. Opt.* **2006**, *45*, 3885-3892.
4. N. Malagnino, G. Pesce, A. Sasso and E. Arimondo, *Opt. Commun.* **2002**, *214*, 15-24.
5. M. Dienerowitz, M. Mazilu and K. Dholakia, *J. Nanophoton.* **2008**, *2*, 021875.
6. L. Tong, V. D. Milijković and M. Käll, *Nano Lett.* **2010**, *10*, 268-273.
7. M. E. J. Friese, T. A. Nieminen, N. R. Heckenberg and H. Rubinsztein-Dunlop, *Nature* **1998**, *394*, 348-350.
8. M. E. J. Friese and H. Rubinsztein-Dunlop, *Appl. Phys. Lett.* **2001**, *78*, 547-549.
9. K. Miyakawa, H. Adachi and Y. Inoue, *Appl. Phys. Lett.* **2004**, *84*, 5440-5442.

Chapter 4. Radiation Pressure Induced Hierarchical Structures of Liquid Crystalline Two-dimensional Materials

In this Chapter, laser beam was irradiated to a liquid crystalline niobate nanosheet colloid with a concentration of 5 g/L.

4-1. Laser Induced Large Orientation Structure of Nanosheets at a Periphery of a Focal Point

Orientation change of a niobate nanosheet liquid crystal was observed with a polarized optical microscope while irradiating a linearly polarized laser beam. The polarized optical microscope images are shown in Figure 4-1. The image before laser irradiation was dark (Figure 4-1 (a)), which indicates the homogeneous orientation of nanosheets with their in-plane perpendicular to the propagation direction of the incident laser beam in the thin-layer cell (see Appendix B).[1,2] Hereafter, such an orientation of nanosheets is referred as “perpendicular orientation”. When the laser beam was irradiated, a birefringent spot appeared immediately at a focal point (Figure 4-1 (b) and Figure 4-2 (a)). After irradiating the laser beam for 15 s, a circularly textured additional birefringence area appeared at the periphery of the birefringence spot as observed at the focal point

(Figure 4-1 (c)). The birefringence indicates the orientation of nanosheets with their in-plane direction parallel to the propagation direction of the incident laser beam (see Appendix B).[1,2] Hereafter, such an orientation of nanosheets is referred as "parallel orientation". Therefore, the appearance of birefringence indicates that the orientation change of the nanosheets occurred at the focal point and the periphery of the focal point under laser irradiation. Although the brightness of the additional area increased gradually until 120 s (Figures 4-1 (c)–(e)), its 110-μm diameter, which was 370 times larger than that of the focal point, was almost constant (see contrast-adjusted images in Figures 4-2).

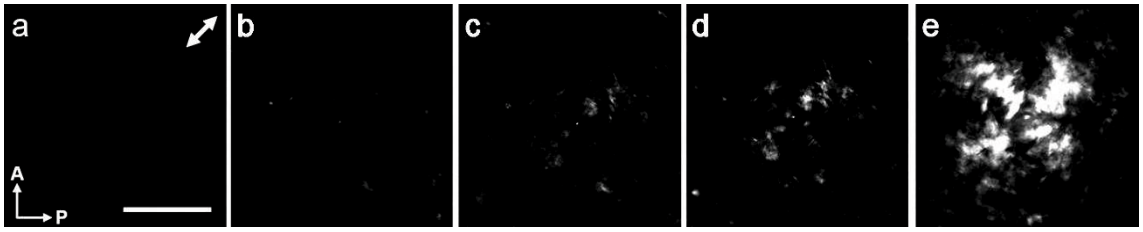

Figure 4-1. Polarized optical microscope images of a liquid crystalline niobate nanosheet colloid (a) before laser irradiation and (b) at 2 s, (c) 15 s, (d) 40 s, and (e) 120 s after laser irradiation. The double arrow indicates the polarization direction of the incident laser beam. The scale bar denotes 50 μm.

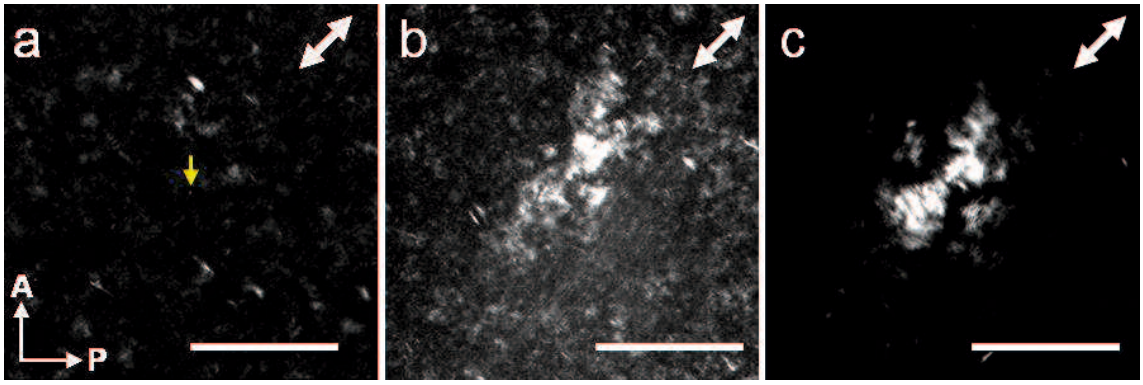

Figure 4-2. Contrast-adjusted polarized optical microscope images of a liquid crystalline niobate nanosheet after (a) 2 s, (b) 15 s, and (c) 40 s of continuous laser irradiation. The double arrows indicate the polarization direction of the incident laser beam. The yellow arrow points to the position of the focal point. The scale bar denotes 50 μm.

A parallel orientation that was induced by laser irradiation was also observed using a bright-field optical microscope. The bright-field optical microscope images are shown in Figure 4-3. The image before laser irradiation was featureless (Figure 4-3 (a)). This is consistent with the perpendicular orientation of nanosheets in the cell. After laser irradiation for 2 s, the image was the same as that before irradiation (Figure 4-3 (b)). However, the magnified image, which is shown in Figure 4-4 (a), demonstrates the presence of nanosheets in parallel orientation, which is the orientation along the polarization direction of the incident laser beam, at the focal point as evidenced by the appearance of line-shaped objects. The size of the domain of nanosheets in a parallel orientation increased gradually during laser irradiation. After laser-beam irradiation for 120 s, the domain diameter reached 15 μm, which was 50 times larger than the focal-point diameter (Figure 4-4 (b)). After laser-beam irradiation for 40 s, another domain, which corresponds to the circularly textured additional birefringence area, appeared gradually at the periphery of the focal point (Figure 4-3 (d)). In this domain, nanosheets in a parallel orientation formed a tree-ring-like texture with a diameter that increased to

80 μm after laser irradiation for 120 s (Figure 4-3 (e)). This size was 270 times larger than the focal-point diameter. Such a large tree-ring-like texture is not generated in an isotropic nanosheet colloid as described in Chapter 3.

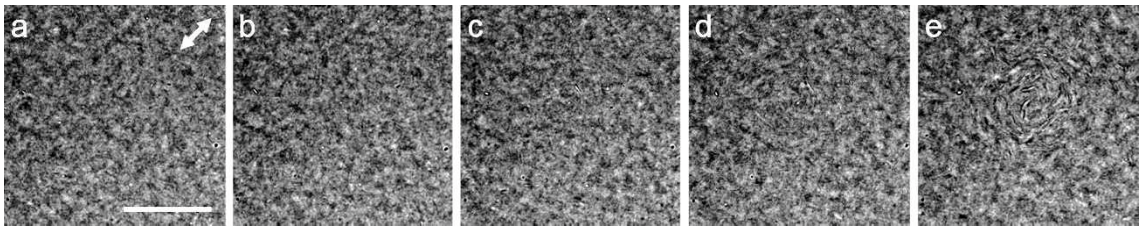

Figure 4-3. Bright-field optical microscope images of a liquid crystalline niobate nanosheet colloid (a) before laser irradiation and (b) at 2 s, (c) 15 s, (d) 40 s, and (e) 120 s after laser irradiation. The double arrow indicates the polarization direction of the incident laser beam. The scale bar denotes 50 μm.

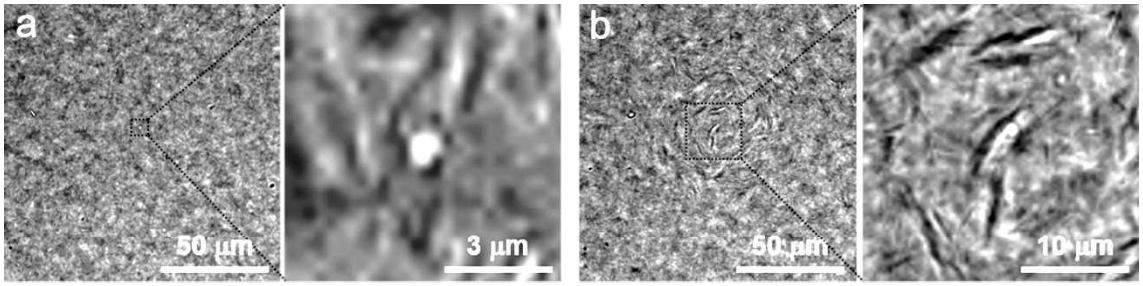

Figure 4-4. Bright-field optical microscope images magnified at the focal point of those after (a) 2 s and (b) 120 s of continuous laser irradiation.

Figure 4-5 shows polarized optical microscope images of the liquid crystalline niobate nanosheet colloid (5 g/L) that was irradiated by rotating the polarization direction of the laser beam. A birefringent spot at the focal point was influenced significantly by the polarization direction of a laser beam. The spot was observed only when the polarization direction of the incident laser beam was nonparallel to the polarizer or analyzer of the microscope. However, the size and brightness of the circularly textured periphery of the focal point was unaffected by the polarization direction.

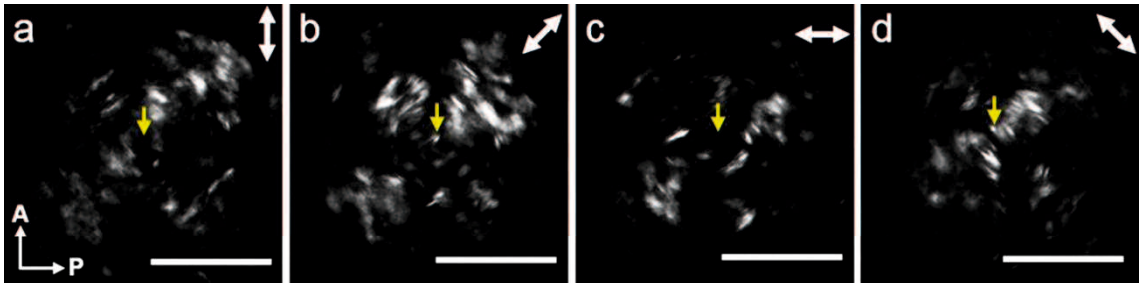

Figure 4-5. Polarized optical microscope images of a liquid-crystalline niobate nanosheet colloid when the polarization direction of a laser beam was rotated. The double arrows indicate the polarization direction of the incident laser beam. The yellow arrows point to the position of the focal point. The scale bar denotes 50 μm.

As described above, when the laser beam was irradiated to a liquid crystalline niobate nanosheet colloid, the nanosheet orientation changed from perpendicular to parallel with respect to the propagation direction of the laser beam. This orientation change is ascribed to a scattering force of the irradiated laser beam. The magnitude of the scattering force that is applied to an object is proportional to the number of photons that irradiated the object.[3] The irradiated area where a nanosheet exists in a perpendicular orientation (1.6 μm×1.6 μm) is 1000 times larger than that where a nanosheet exists in parallel orientation (1.6 μm×1.6 nm). Therefore, the scattering force that is applied to a nanosheet in a perpendicular orientation should be 1000 times larger than that applied to a nanosheet in a parallel orientation. When the shape anisotropy, and thus the anisotropy of the scattering force that is applied to an object, is significant, such as 1D materials, it has been reported that the anisotropic materials orient their long-axis parallel to the propagation direction of the incident laser beam to minimize the applied scattering force.[4] The large anisotropy of the scattering force that is applied to the nanosheet should also result in a parallel orientation.

The domain that was formed at the focal point is ascribed to the scattering force and polarization direction of the electric field of the incident laser beam. In this domain, nanosheets aligned along the polarization direction of the incident laser beam. This alignment is rationalized by a previous study of electric alignment of liquid crystalline niobate nanosheets.[1,2] The trapped and electrically aligned nanosheets form a core around which nanosheets are assembled to produce the domain. However, the size is restricted to ~15 μm.

The domain at the periphery of the focal point is ascribed only to the scattering force. In this domain, a tree-ring-like nanosheet alignment that is independent of the laser polarization was observed. This result indicates that the orientation change is not caused by a gradient force. Based on a cylindrical alignment of nanosheets, the origin of this orientation change should be a scattering force that is applied to objects, and which corresponds to a Gaussian distribution of the radiation intensity of the irradiated laser beam.

4-2. Expected Mechanism of Construction of Hierarchical Structure Induced by Laser Radiation Pressure

Figure 4-6 shows a schematic representation of the orientation change. Before laser irradiation, the nanosheets are perpendicular to the propagation direction of the laser beam, but they are not strictly oriented (Figure 4-6 (a)). With laser irradiation, the nanosheets at the highest irradiance region are trapped rapidly to form a domain with a direction that is dependent on the polarization direction of the laser beam (Figure 4-6 (b), the domain at the focal point is indicated by brown nanosheets). At the same time, nanosheets in a region where the scattering force is sufficient for a laser-induced orientation change (near to the focal point, indicated as a yellow background area) also start the orientation change, which proceeds gradually. Nanosheets, even at the outside of the beam path, are aligned because of the liquid crystallinity of the sample. Nanosheets near the already aligned nanosheets are drawn and aligned with nanosheet-nanosheet interactions. This process increases the population of aligned nanosheets in a cylindrical region around the beam path to form the peripheral domain (Figures 4-6 (c) and (d)). Finally, nanosheets around the beam path are aligned sufficiently to provide a well-grown peripheral domain (Figure 4-6 (e)). At this stage, the domain at the focal point with nanosheets that is oriented along the polarization direction is surrounded by nanosheets that are oriented into tree rings (cross-sectional image; Figure 4-6 (f)). This model is consistent with textural changes that are observed by the polarized and bright-field microscope images. In addition, this model is also consistent with the power dependence of the texture size. When a laser beam of 100 mW was used, namely, the scattering force was enhanced, the diameter of the circular textured area grew to 200 μm (Figure 4-7).

The contribution of thermal flow can be ruled out. The 20-mW laser-power irradiation

was smaller by an order of magnitude than used in conventional optical manipulation studies in which thermal flow occurred. In addition, the sample consists of nanosheets and water does not absorb light at 532 nm.

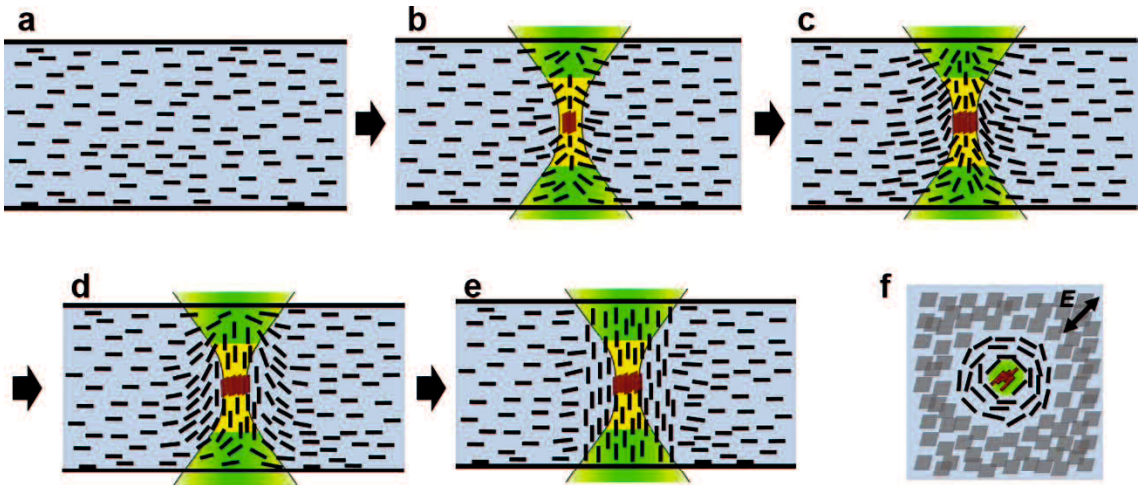

Figure 4-6. Schematic representation of orientation change of niobate nanosheets by laser radiation pressure (a-e). Cross-sectional image of Figure 4-6e in the focal plane is shown in Figure 4-6f. Nanosheets trapped at the focal point are indicated in brown. Green and yellow regions denote a beam path and an area with a high irradiance, respectively.

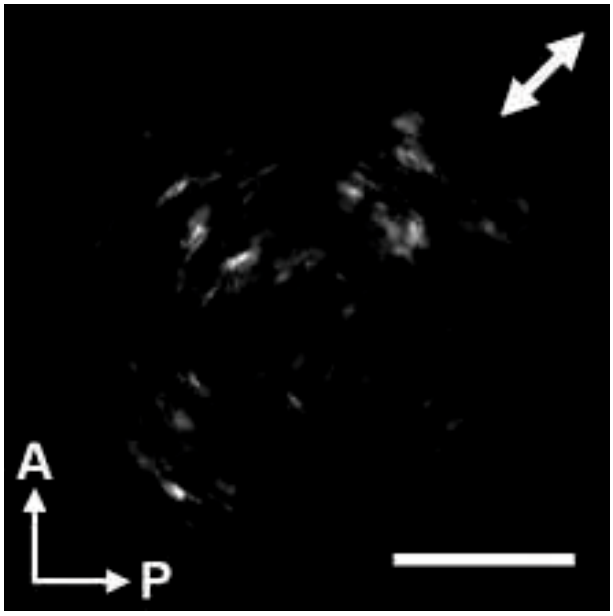

Figure 4-7. Polarized optical microscope image of a liquid-crystalline niobate nanosheet colloid when a laser beam of 100 mW was irradiated for 120 s after laser irradiation. The double arrow indicates the polarization direction of the incident laser beam. The scale bar denotes 50 μm.

4-3. Conclusion

In this Chapter, the local and on-demand hierarchical structure of liquid crystalline nanosheet constructed by combining of the laser radiation pressure and interparticle interactions based on the liquid crystallinity of the nanosheets has been discussed. When a linearly polarized laser beam was irradiated to the niobate nanosheet liquid crystal, local hierarchical structures were generated on-demand. The structure consisted of two domains. One was found close to the focal point. The size of the domain was 15 μm, which was 50 times larger than that of the focal point. In this domain, nanosheets oriented their in-plane parallel to the propagation direction and the polarization direction of the incident laser beam. This behavior was essentially the same as the orientation manipulation of a colloidal nanosheet revealed in Chapter 3. The other domain was found at the periphery of the domain close to the focal point. The diameter of the domain was more than 110 μm, which was 370 times larger than that of the focal point. In the domain, nanosheets which oriented their in-plane direction parallel to the propagation direction of the incident laser beam formed a tree-ring-like texture.

In previous papers concerned with hierarchical structures constructed by the laser radiation pressure, a high power laser beam of 1 W is required to construct them (see Appendix C). This laser power is too high to manipulate soft materials non-invasively. However, in this study, hierarchical structures were constructed at extremely low laser power due to the aid of interparticle interactions of liquid crystalline nanosheets. In addition, the size of hierarchical structures constructed in this study was much larger than that reported previously due to the large excluded volume of nanosheets and thus the large interparticle interaction between liquid crystalline nanosheets.

References

1. T. Nakato, Y. Nono, E. Mouri and M. Nakata, *Phys. Chem. Phys. Chem*. **2014**, *16*, 955-962.
2. T. Nakato, K. Nakamura, Y. Shimada, Y. Shido, T. Houryu, Y. Iimura and H. Miyata, *J. Phys. Chem. C* **2011**, *115*, 8934-8939.
3. E. Hecht in *Optics*, Addison Wesley Longman, Inc., the United States, **1998**, pp. 55-57.
4. L. Tong, V. D. Milijković and M. Käll, *Nano Lett.* **2010**, *10*, 268-273.

Chapter 5. Conclusion

In this study, optical manipulation of 2D plate-like particles has been realized for the first time. Based on the observations, the mechanism of optical trapping and orientation manipulation of 2D plate-like particles has been revealed.

When irradiating a linearly polarized laser beam to randomly dispersed nanosheets, a nanosheet was trapped at the focal point to orient its in-plane direction parallel to the propagation direction of the incident laser beam. In addition, the trapped nanosheet aligned along the polarization direction of the incident laser beam and rotated with the rotation of the polarization direction. A unidirectional alignment of a nanosheet was realized by one external force of a linearly polarized laser beam.

When a circularly polarized laser beam was irradiated, the trapped nanosheet was rotated continuously by the spin angular momentum of the circularly polarized laser beam. The rotation direction of the trapped nanosheet was switchable by controlling the direction of the circularly polarized laser beam.

When a laser beam was irradiated to a liquid crystalline nanosheet colloid, a hierarchical structure on the scale of 100 μm was found to be formed. The structure consisted of two domains. One was found close to the focal point. The size of the domain was 15 μm, which was 50 times larger than that of the focal point. In this domain,

nanosheets oriented their in-plane direction parallel to the propagation direction and the polarization direction of the incident laser beam. The other domain was a giant tree-ring-like texture of more than 100 μm formed at the periphery of the domain close to the focal point. Thus, nanosheets were found to form such a hierarchical structure owing to a large excluded volume characteristic to liquid crystalline nanosheets.

2D plate-like particles have been attracted considerable attention due to novel functionalities arising from their high anisotropy. In order to maximize the functionality, a methodology that enables the local and on-demand orientation manipulation of 2D plate-like particles has strongly desired. Optical manipulation of 2D plate-like particles established in this study should provide a powerful methodology for realizing required orientation of 2D plate-like particles and therefore should expand the application of 2D plate-like particles.

Appendix

A. Inorganic Nanosheets[1]

Inorganic nanosheets are 2D plate-like materials with thickness of ~1 nm and lateral length in the range of several to thousands of times larger than their thickness. Therefore, the inorganic nanosheets have very high aspect ratio and thus large excluded volumes in the colloidal state. Inorganic nanosheets are prepared by exfoliation of inorganic layered crystals and have attracted great attention due to their high anisotropic shape. A variety of nanosheets have been prepared and examined as building blocks of functional nanoassemblies. For example, layer-by-layer assemblies,[2] thin films,[3] porous solids,[4] inorganic-polymer hybrids,[5] and so forth have been fabricated.

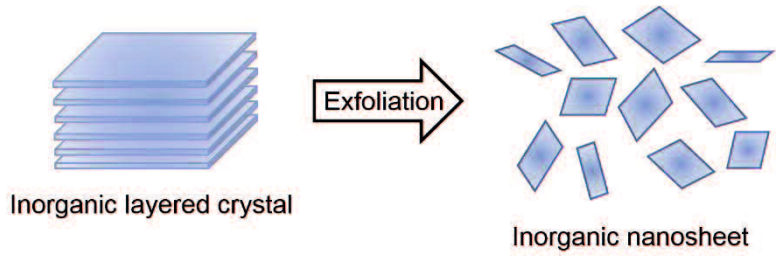

Figure A-1. Schematic representation of inorganic layered crystals and inorganic nanosheets.

B. Liquid Crystalline Nanosheet Colloids[6,7]

Inorganic nanosheets prepared by exfoliation of inorganic layered crystals are obtained as a nanosheet colloid because the exfoliation is usually carried out in water. Because inorganic nanosheets have large excluded volumes, freedom of rotational motion of the nanosheets in the nanosheet colloid is restricted at a high nanosheet concentration. Such a system can be stabilized when some nanosheets have orientation order because entropy in the system is maximized by the acquirement of translational entropy instead of loss of rotational entropy.[8] Therefore, some of the inorganic nanosheet colloids exhibit lyotropic liquid crystallinity by optimization of the concentration, the size of the nanosheet and so forth.

Among liquid crystalline nanosheet colloids, those prepared by exfoliation of layered niobate has been well investigated. Niobate nanosheets are aligned in a lamellar manner with a basal spacing of several tens of micrometers in the liquid crystalline state.[9] Liquid crystalline domains grow through self-assembly by incubating liquid crystalline nanosheet colloid at room temperature to reach a sub-millimeter size.[10] The nanosheets respond to an external field, such as a shear force and an electric field.[11,12] Hierarchical macroscopic structures can be formed in the liquid crystalline nanosheet colloids by combining domain growth and an electric field.[10,13] With these methods, a colloid sample is organized in the same manner in the entire sample.

In general, orientations of nanosheets in the hierarchical macroscopic structures or the liquid crystalline domains have been confirmed with a polarized optical microscope.[10] Specifically, the orientation of nanosheets has been predicted based on the relationship between an orientation of nanosheets and the birefringence observed with a polarized optical microscope. This situation is schematically represented in Figure B-1. When nanosheets orient their in-plane direction perpendicular to the propagation direction of illuminated light, no birefringence is observed (Figure B-1(a)). On the other hand, when nanosheets orient their in-plane direction parallel to the propagation direction of the illuminated light, birefringence is observed (Figure B-1 (b)). Here, it should be noted that when nanosheets which orient their in-plane direction parallel to the propagation direction of the illuminated light are along polarization directions of a polarizer or an analyzer, no birefringence is observed.

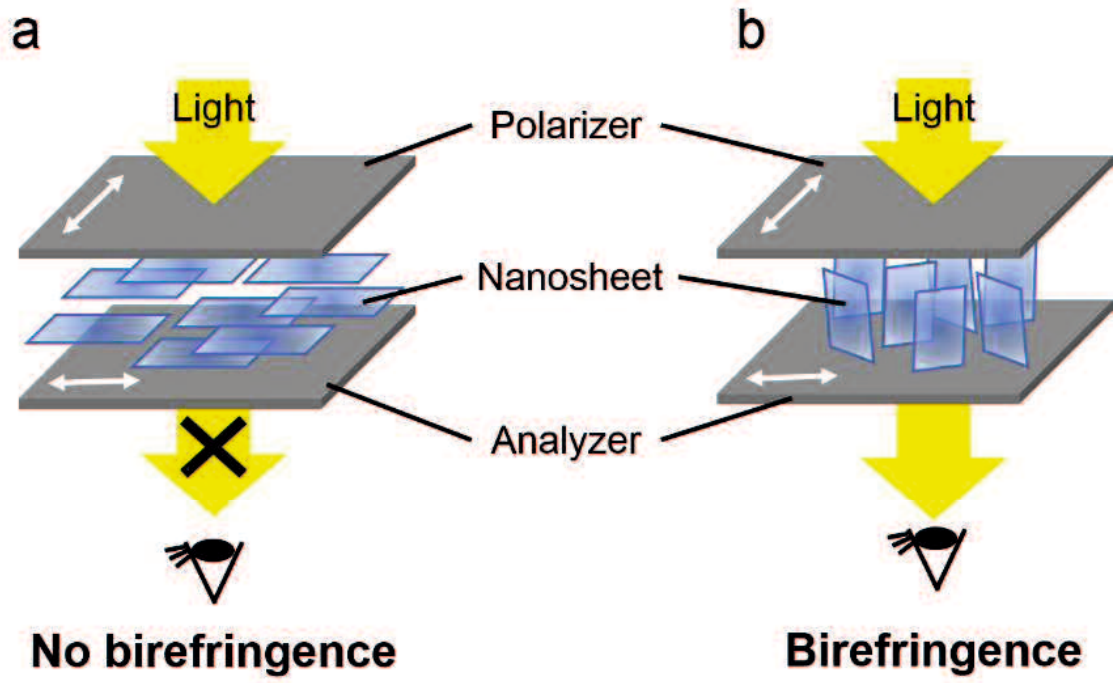

Figure B-1. The relationship between an orientation of nanosheets and observed birefringence in polarized optical microscope observations. The double arrows indicate the polarization direction. When nanosheets orient their in-plane direction perpendicular to illuminated light between a polarizer and an analyzer which are orthogonal, no birefringence is observed (a). On the other hand, when nanosheets orient their in-plane direction parallel to illuminated light, birefringence is observed (b).

C. Hierarchical Structures Induced by Laser Radiation Pressure

Colloidal particles are typically trapped only at a focal point by the radiation pressure of a tightly focused laser beam. However, very recently, it is reported that hierarchical structures are constructed not only at a focal point but also at the periphery of the focal point by the use of the laser radiation pressure. Currently, making use of either intermolecular interaction or interface is the methodology for construction of a hierarchical structure that is larger than a focal point by laser irradiation. For example, in 2011, Usman et al. reported that a laser beam of 1.2 W that was focused on a nematic liquid crystal, 4'-pentyl-4-cyanobiphenyl yielded a new domain at around the focal point with the diameter size of 24 μm, which was twenty four times larger than the size of the focal point, 1 μm.[14] The formation of such a hierarchical structure was attributed to the re-orientation of liquid crystalline molecules as determined by the balance between the generated optical and preexisting elastic torque of the nematic liquid crystal,[15] based on the intermolecular interaction of the liquid crystal and the laser radiation pressure.

Construction of hierarchical structures of colloidal particles is limited at interfaces. For example, in 2016, Wang et al. reported that colloidal polystyrene particles was assembled at an air-liquid interface to construct a closely packed hierarchical structure by irradiation of a tightly focused laser beam.[16,17] When irradiating a focused laser beam of 1.4 W on an air-liquid interface to the colloidal particles with 200 nm, they are assembled

at the focal point as is the conventional optical manipulation at the first stage. Continuous irradiation of the laser irradiation grew the assembly toward the periphery of the focal point to construct a closely packed hierarchical structure with an assembly size of 20 μm, which was twenty times larger than the size of the focal point, 1 μm. Furthermore, in 2016, Kudo et al. reported that, at an interface between their colloidal solution and the glass substrate, colloidal polystyrene particles were assembled to construct a hierarchical structure with horns by irradiation of a tightly focused laser beam.[18] When irradiating a focused laser beam of 1.4 W on the interface to the colloidal particles with the size of 500 nm, a closely packed hierarchical structure larger than the focal point was constructed at the interface as reported by Wang et al.[16,17] Continuous laser irradiation formed horns like particle assembly from the hierarchical structure and became longer. The total size of the hierarchical structure with horns was 30 μm, which was thirty times larger than the size of the focal point, 1 μm. The construction of these hierarchical structures which consist of assembled colloidal particles was attributed to multiple scattering between the colloidal particles in two-dimensions. These results suggest that the laser radiation pressure of colloids evolves certain hierarchical structures that span from the focal point to the periphery at interfaces. However, reports on hierarchical structures that are larger than those of the focal points in colloidal system are limited to the above examples.

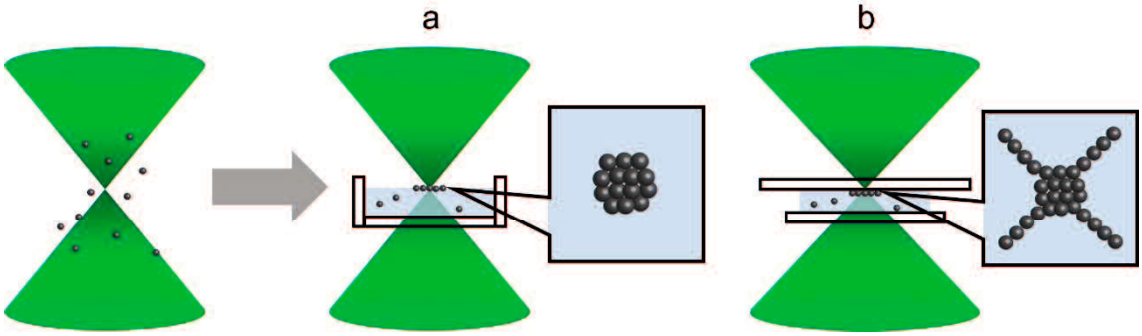

Figure C-1. Schematic representation of hierarchical structures which consist of assembled polystyrene particles constructed (a) at an air-liquid interface reported by Wang et al.[16,17] and (b) at an interface between a colloidal solution and the glass substrate reported by Kudo et al.[18]

References

1. T. Nakato, J. Kawamata and S. Takagi in *Inorganic Nanosheets and Nanosheet-Based Materials* (Eds.: T. Nakato, J. Kawamata and S. Takagi), Springer, Japan, **2017**, pp. 3-32.
2. R. A. Schoonheydt and Y. Umemura in *Inorganic Nanosheets and Nanosheet-Based Materials* (Eds.: T. Nakato, J. Kawamata and S. Takagi), Springer, Japan, **2017**, pp. 40-41.
3. R. A. Schoonheydt, *Appl. Clay Sci.* **2014**, *96*, 9-21.
4. T. Nakato in *Inorganic Nanosheets and Nanosheet-Based Materials* (Eds.: T. Nakato, J. Kawamata and S. Takagi), Springer, Japan, **2017**, pp. 80-81.
5. A. Usuki, N. Hasegawa, M. Kato and S. Kobayashi in Inorganic Polymeric Nanocomposites and Membranes, Springer, Germany, **2005**, pp. 135-195.
6. N. Miyamoto, Y. Ohsedo and T. Nakato in *Inorganic Nanosheets and Nanosheet-Based Materials* (Eds.: T. Nakato, J. Kawamata and S. Takagi), Springer, Japan, pp. 201-262.
7. T. Nakato and N. Miyamoto, *Materials* **2009**, *2*, 1734-1761.
8. L. Onsager, *Ann. N. Y. Acad. Sci.* **1949**, *51*, 627-659.
9. D. Yamaguchi and N. Miyamoto, T. Fujita, T. Nakato, S. Koizumi, N. Ohta, N. Yagi and T. Hoshimoto, *Phys. Rev. E* **2012**, *85*, 011403.
10. T. Nakato, Y. Nono, E. Mouri and M. Nakata, *Phys. Chem. Chem. Phys.* **2014**, *16*, 955-962.
11. N. Miyamoto, and T. Nakato, *J. Phys. Chem. B* **2004**, *108*, 6152-6159.
12. T. Nakato, K. Nakamura, Y. Shimada, Y. Shido, T. Houryu, Y. Iimura and H. Miyata, *J. Phys. Chem. C* **2011**, *115*, 8934-8939.
13. T. Nakato, Y. Nono and E. Mouri, *Colloid Surf., A* **2017**, *522*, 373-381.
14. A. Usman, T. Uwada and H. Masuhara, *J. Phys. Chem. C* **2011**, *115*, 11906-11913.
15. I. C. Koo, T. H. Liu and P. Y. Yan, *J. Opt. Soc. Am. B* **1987**, *4*, 115-120.
16. S. -F. Wang, K. Yuyama, T. Sugiyama and H. Masuhara, *J. Phys. Chem. C* **2016**, *120*, 15578-15585.
17. S. -F. Wang, T. Kudo, K. Yuyama, T. Sugiyama and H. Masuhara, *Langmuir* **2016**, *32*, 12488-12496.
18. T. Kudo, S.-F. Wang, K. Yuyama and H. Masuhara, *Nano Lett.* **2016**, *16*, 3058-306.